



Online droplet monitoring in inkjet 3D printing using catadioptric stereo system

Tianjiao Wang^a , Chi Zhou^a , and Wenyao Xu^b 

^aDepartment of Industrial and Systems Engineering, University at Buffalo, Buffalo, NY, USA; ^bDepartment of Computer Science and Engineering, University at Buffalo, Buffalo, NY, USA

ABSTRACT

Inkjet 3D printing is becoming one of the most disruptive additive manufacturing technologies, due to its unique capability of precisely depositing micro-droplets of multi-functional materials. It has found widespread industrial applications in aerospace, energy and health areas by processing multi-functional metal-materials, nano-materials, and bio-materials. However, the current inkjet 3D printing system still suffers from a low production quality issue, due to low process reliability caused by the complex and dynamic droplet dispensing behavior. Due to the challenges in terms of efficiency, accuracy, and versatility, robust droplet monitoring and process inspection tools are still largely unavailable. To this end, a novel catadioptric stereo system is proposed for online droplet monitoring in an inkjet 3D printing process. In this system, a regular industrial CCD camera is coupled with a flat mirror and magnification lens system to capture the tiny droplet images to detect the droplet location in 3D space. A mathematical model is formulated to calculate the droplet location in 3D world space from 2D image space. A holistic hardware and software framework is constructed to evaluate the performance of the proposed system in terms of resolution, accuracy, efficiency, and versatility, both theoretically and experimentally. The results show that the proposed catadioptric stereo system can achieve single micron resolution and accuracy, which is one-order-of-magnitude higher than the 3D printing system itself. The proposed droplet location detection algorithm has low time complexity, and the detection efficiency can meet the online monitoring requirement. Multi-facet features including the droplet location and speed can be effectively detected by the presented technique. The proposed catadioptric stereo system is a promising online droplet monitoring tool and has tremendous potential to enable trustworthy quality assurance in inkjet 3D printing.

ARTICLE HISTORY

Received 5 December 2017
Accepted 23 September 2018

KEYWORDS

3D printing; inkjet; catadioptric stereo; online monitoring; quality assurance

1. Introduction

1.1. Background

Three-dimensional (3D) printing or additive manufacturing is a disruptive advanced manufacturing technology that can directly fabricate physical objects from digital models through spatially depositing energy or materials (Gao *et al.*, 2015). Inkjet 3D printing is one very promising technology among many others including Fused Deposition Modelling (FDM) (Sun *et al.*, 2018; Wang *et al.*, 2017a), Stereolithography (SLA) (Zhou *et al.* 2009; Zhou *et al.*, 2013) and Selective Laser Sintering (Gibson *et al.*, 2010). By precisely depositing micro-scale droplets of various different materials in the same build, inkjet 3D printing can achieve many functionalities, including functionally graded material printing, and digital material fabrication (Gibson *et al.*, 2010), which have found widespread applications in aerospace, biomedical and energy areas (Wohlers, 2016). To name a few, *bio-materials* have been widely used to inkjet print tissues and organs with multiple types of cells and extracellular-matrix for biomedical and health applications (Mironov *et al.*, 2003; Bose *et al.*, 2013). Very recently,

nano-materials such as graphene, dichalcogenides and nano-wires have been inkjet 3D printed into multi-functional products (supercapacitors, batteries, catalysis, sensors) for energy, environment and electronics applications (Zhang *et al.*, 2016; Yan *et al.*, 2017; Zhang *et al.*, 2017). An innovative metal 3D printing company called Vader System Inc. utilized inkjet printing technology to 3D print metal-materials by melting metal filament and propelling liquefied metal through inductive force in a drop-on-demand manner, which found wide applications in aerospace, defense and automobile areas (Potter, 2017; Wang *et al.*, 2018).

Though tremendous efforts and progress have been made in the promising inkjet 3D printing process during the past few years, as an emerging technology, there are still multiple challenges which handicap its large-scale commercialization in practice. The major obstacle is that the inkjet process still suffers from low production quality issues, due to the low process reliability and product accuracy (Gibson *et al.*, 2010; Wang, Kwok & Zhou, 2017c). Due to the complex and dynamic droplet dispensing process, robust inspection and quality assurance tools are still largely unavailable. More specifically, the droplet size has to be very small for high

printing resolution, thus droplets are vulnerable to many uncertain factors, such as vibration, material inhomogeneity, air dynamics and temperature fluctuations. In the layer-by-layer additive process, if the process drifts (droplet location, speed, and size) cannot be corrected in a timely manner, defective droplets will deteriorate the geometric integrity (dimension, surface finishing) and functional integrity (fatigue, strength) of the printed part. Consequently, the low-quality and defective parts will lead to reduced product value or material waste, and will even seriously affect the structural health conditions and infrastructural integrity of many important engineering systems, especially for mission-critical applications.

1.2. Challenge and related work

An effective online droplet monitoring system plays a vital role in quality assurance of 3D printing. A trustworthy monitoring system can assist not only in-process diagnosis for human-in-loop 3D printing processes, but also enable subsequent closed-loop control-based autonomous manufacturing systems. During the past decade, tremendous effort and progress have been made to develop advanced sensing technologies for the monitoring of 3D printing processes. To name a few, the heterogeneous sensor array has been studied on the FDM 3D printer to detect the printing defects (Rao *et al.*, 2015) and surface texture information captured by the digital microscope was used for monitoring the printing condition (Liu *et al.*, 2017). Cameras have been used to monitor the height of the 3D printed part (Mazumder and Voelkel, 1995; Mazumder *et al.*, 2000). Specifically, the CCD camera used in this work is a Pulnix TM-745, and it operates at 1/60 and 1/125 seconds shutter-speed and produces 30 frames per second. Nevertheless, this method can only provide two-dimensional (2D) information of the printed parts, which is not sufficient for monitoring high-accuracy inkjet 3D printing. For the SLA-based 3D printing process, Xu and Chen (2017) used a thermal camera to study the shape deformation and also used a 3D scanner-based close-loop framework for shape deformation control (Xu *et al.*, 2017). A vision-based method was also used to monitor the 3D printing process (Cheng and Jafari, 2008), but this method focused on the continuous deposition process, which is not applicable to high-throughput inkjet 3D printing. Faes *et al.* (2016) presented a way using a laser to obtain the 3D structure of printed parts; however, in-process information cannot be revealed, which is the key to the success of the 3D printing process. Temperature and thermal image-related monitoring technologies have been widely developed and studied for Direct Metal Laser Sintering (DMLS) machines. Salehi and Brandt (2006) developed a LabVIEW-based system to control the laser cladding temperature. Hu and Kovacevic (2003) used an infrared image to control the melt pool, and Toyserkani and Khajepour (2006) focused on height and angle of the clad. These methods are effective for the DMLS 3D printing process, but they are not suitable for the inkjet 3D printing process where the droplet behavior is the primary decision

factor in the process reliability and product quality. As for the quality improvement in inkjet printing, Zhou and Chen (2009a) developed a simulator for the control of droplet jetting in the piezo-based multi-jet modeling process to increase the surface finishing of the printed part.

Droplet location is one of many factors including droplet size, shape, speed, and stability in inkjet 3D printing, and has a direct influence on the quality of printing. For example, droplets that land at undesired locations can cause defects or even failure of the whole printed part (Wang *et al.*, 2017b). As such, the location of a droplet is the major focus of this work. Using a single camera to monitor the inkjet printing process can provide useful information related to the jetting behavior including the number of satellites, droplet size, etc. (Wang, Kwok & Zhou, 2017c), however, the location of a 3D droplet cannot be obtained from a single camera in previous studies. In this research, we will mainly focus on the monitoring of the droplet location. There are four major challenges to bring online monitoring technologies to an inkjet printing system:

1. High accuracy. The process monitoring system should be accurate enough and at least up to the physical resolution of the 3D printers to enable high-fidelity quality control. However, the droplet size in inkjet 3D printing systems is measured in microns (a typical droplet diameter is between 50 μm and 100 μm (Gao and Sonin, 1994; Bose *et al.*, 2013; Zhang *et al.*, 2016)), and it is very challenging to design a non-invasive monitoring system that can reach single micron resolution.
2. Real-time monitoring. The deposition rate in inkjet printing is typically measured as being between 100 and 1000 droplets per second, the monitoring system should be fast enough to capture the droplets before the defective ones land onto the substrate. Therefore, real-time in-process monitoring, as opposed to post-process examination, is desired for trustworthy quality assurance.
3. Multi-dimensional information. The monitoring system should be able to capture multi-dimensional data from the jetting process and extract critical information including the droplet location and speed in 3D space. However, the commonly used imaging systems can only capture incomplete droplet information in reduced 2D space.
4. Easy to deploy and low cost. The inkjet printing head is typically installed close to the substrate to ensure high printing quality (the fly distance of a droplet is usually several millimeters (Zhang *et al.*, 2017)), and the compact space imposes the challenge to conveniently deploy the monitoring system. In addition, to promote its scale-up applications, the monitoring system should be cost-effective, which excludes prohibitively expensive sensing systems.

Ultimately, the most challenging aspect of an online monitoring system for droplets is that all the above challenging criteria are at odds with each other. For example, “multi-dimensional information” often requires a time-consuming sophisticated process of data collection and analysis, while “real-time monitoring” requires the monitoring

process to be efficient, oftentimes by sacrificing the “accuracy” and “cost.” There is an urgent need to develop an effective inspection tool to precisely and efficiently detect, analyze and localize the droplet to enable quality assurance and certification, and ultimately solve the low-quality issues for inkjet 3D printing applications.

1.3. Motivation and proposed approach

As a powerful non-invasive inspection tool, the image-based system (e.g., high-speed video camera) has been widely used for process monitoring (Wang, Kwok & Zhou 2017c); however, it can only capture the incomplete information in 2D space. On the other hand, a multiple-image-based system is the essential component of 3D scanning tools for scene reconstruction (Huang, 2016; Tootooni *et al.* 2017); however, they are mainly used for macro-scale applications and cannot provide the required accuracy and processing speed for micro-droplet monitoring applications. Motivated by the unique properties of imaging-based monitoring systems, we propose a catadioptric stereo system by seamlessly integrating reflection, imaging, and microscope-based optical systems, to monitor the location of 3D droplets with high accuracy and fast processing speed. The hypothesis is that multiple synchronized and magnified 2D images can provide an effective non-invasive monitoring tool to efficiently and precisely detect and localize the droplet in 3D space. To the best of our knowledge, the proposed system represents one of the most effective technologies for droplet online monitoring in inkjet 3D printing.

The proposed catadioptric stereo system has the potential to fundamentally address the aforementioned challenges. The underlying rationale is listed as follows:

1. High accuracy. A magnification lens system is added to the traditional image system such that the physical detection resolution can be increased by the magnitude of the magnification system.
2. Real-time monitoring. The fast processing speed is radically increased in two ways. First, the proposed monitoring system only focuses on the image area occupied by the allowable droplet locations, which is measured in less than one millimeter. Therefore, compared with the traditional micro-scale application-based 3D scanning systems, the proposed system requires a much lower computational cost. Second, the traditional 3D scanning system processes thousands or millions of data points to reconstruct the high-fidelity 3D object (Chen *et al.*, 2013). In the proposed technique, only specific properties of the droplet have to be detected. For example, to detect a droplet’s location, only one data point (the centroid of the droplet) should be processed. This also applies to other properties such as droplet speed and size (Rajagopalan and Chaudhuri, 1997; Favaro *et al.*, 2003). Therefore the complexity is reduced from $O(n)$ to $O(1)$, where n is the number of data points for traditional 3D scanning.
3. Multi-dimensional information. Dual cameras (real camera and virtual camera) are used to capture the droplet, therefore

the 3D information about the droplet (location, speed, size) can be obtained, whereas the traditional monitoring system can only detect information in 2D space.

4. Easy to deploy and low cost. Instead of using two cameras, the proposed system uses one camera and a mirror which serves as a virtual camera. Therefore it can significantly reduce the system cost and make it easier to deploy.

The contributions of this article are summarized as:

1. We proposed a high fidelity micro-droplet monitoring system that opens up a new angle to address the quality issue in inkjet 3D printing. The existing work using cameras can only obtain 2D information about the inkjet’s behavior, whereas the proposed catadioptric system can provide key information about the micro-droplet in 3D space.
2. High efficiency and accuracy of the monitoring system are achieved by utilizing domain knowledge that is specific to the droplet detection in inkjet 3D printing:
 - Dimension reduction. By projecting the point cloud of the 3D droplet surface onto its central location, the time complexity of the droplet location algorithm is reduced from linear to constant.
 - Information densification. By incorporating a optical system for magnification, the monitoring system only focused on the droplet and its vicinity. Compared with the regular optical system which provides a low-resolution image of the droplet, our magnified system can exclude the useless information from the background images and only provide the related information from the droplet image. The high-density information can simultaneously increase efficiency and accuracy.
3. We developed a holistic hardware and software framework to evaluate the performance of the proposed system in terms of resolution, accuracy, efficiency, and versatility both theoretically and experimentally. The results show that the proposed catadioptric stereo system can achieve single micron resolution, which is one order of magnitude higher than the 3D printing system itself.

The remainder of this article is organized as follows. The principles that underpin our approach and a mathematical model of the catadioptric stereo system are introduced in Section 2. Section 3 describes the design and analysis of the online monitoring system. System evaluation including resolution, accuracy, time efficiency and other capabilities are presented in Section 4. Finally, we discuss the future study and conclude in Section 5.

2. Catadioptric stereo droplet location detection system

2.1. Catadioptric stereo model

It should be noted that catadioptric stereo is not a brand new technology, and it has been studied since the 1990s

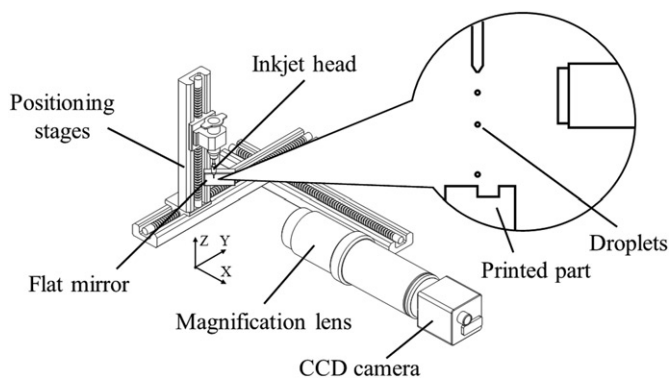


Figure 1. A schematic drawing of the catadioptric stereo system.

(Goshtasby and Gruver, 1993; Inaba *et al.*, 1993; Nene and Nayar, 1998). However, the main purpose of these previous studies was to use multiple images to reconstruct a 3D scene, and very few of them were used to detect and monitor a target location. Jackson *et al.* (2016) presented a catadioptric stereo system to locate a cardiac catheter with a length of 110 mm and at a distance of 6 m. Although that setup is not directly applicable to the detection of tiny objects, the concept shed light on a potentially elegant solution to the problem of the detection of the location of micro-droplets in the inkjet 3D printing process through the modification of an existing catadioptric stereo system.

The major components of the proposed catadioptric stereo system consist of a CCD camera, a mirror, and a magnification lens system. The system structure is briefly shown in Figure 1. The mirror can be adjusted to obtain the best field of view and kept fixed during the calibration and detection process. The angle of the mirror to the camera axis is set at 45° to achieve consistent resolution in the X and Y axes. In a traditional multi-camera-based reconstruction system, the synchronization of the camera shutters needs to be carefully considered. As the droplet flies with a fast speed, if the cameras take images at different time stamps of the same droplet, non-negligible operational errors will be introduced, due to the undesired time delay. In the proposed catadioptric system, the camera takes the real image and the virtual image (reflected by the mirror) at the same time, and this addresses the synchronization issue, which is an important advantage for a precise and efficient monitoring system. In addition, the tiny mirror used in this system has a small footprint and significantly increases the accessibility and makes it easier to deploy the system and reduce the cost compared with a multi-camera design.

Comparing with a traditional catadioptric stereo system for 3D scene reconstruction (Inaba *et al.*, 1993; Gluckman and Nayar, 2002), the proposed stereo system has two unique features that serve the purpose of improving the accuracy and efficiency of the detection process. The first feature is that the proposed system adopts a wider detection angle. In general, the camera has a higher detection resolution and accuracy for the targets placed on the plane perpendicular to the camera direction than along the camera direction. As shown in Figure 2(a), the mirror in our system is placed at an angle of 45° to the camera direction and this allows the target droplet to locate on the

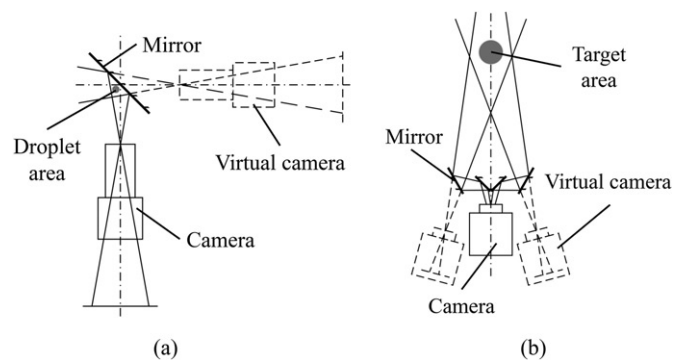


Figure 2. Comparison between (a) our proposed catadioptric stereo system and (b) a traditional system for scene reconstruction.

planes perpendicular to the directions of both the real camera and virtual camera, leading to high resolutions in the directions of both along and perpendicular to the camera. In the traditional scene reconstruction system, the distance between cameras (or virtual cameras) is usually much smaller than the distance between the camera and the target (Inaba *et al.*, 1993; Gluckman and Nayar, 1999). The purpose of such a configuration is to achieve a large detection/reconstruction area with a narrower detection angle; however, a large portion of the target in this configuration is off the perpendicular direction (Figure 2(b)) and this results in a lower detection resolution. The second unique feature is that the proposed system uses a magnification lens system rather than a minification lens system. The tiny droplet is magnified to the scale that the camera image is mapped to all the allowable locations of the jetted droplets, which is measured to be less than 1 mm x 1 mm. The magnified image can significantly increase the resolution and accuracy of the detection system. It should be noted that any droplets outside the allowable range are considered as uncorrectable anomalies, which requires manual operator intervention for corrective action or process diagnosis.

In order to establish the relation between the target location in the 3D world space and its corresponding location in the image space from the cameras, the pinhole model is commonly used in traditional stereo reconstruction systems. Although a magnification lens or microscope is used in the stereo system, studies (Ralis *et al.*, 2000; Ammi, *et al.*, 2005; Figl *et al.*, 2005), a pinhole model can in fact be used for magnification-based optical systems. In our system, though the target and its image in the mirror are both captured by the same camera, it is equivalent to consider these two images are captured by two cameras (a real camera and a virtual camera) with the same intrinsic properties. As such, the catadioptric stereo model formulated in this work is similar to the generally used dual-camera-based 3D scene reconstruction system. More specifically, the following information is required to establish the mapping between the location in world space and the image space: the scene, the camera, and the relative location between the scene and the camera. Typically, the information of the scene itself is limited, and information about the camera (focal length, sensor size, etc.) is usually required to better reconstruct the scene (Hartley and Zisserman 2003). However, if the scene information (e.g., the accurate location of the targets) is available, the calibration and detection can be implemented without knowing the detailed

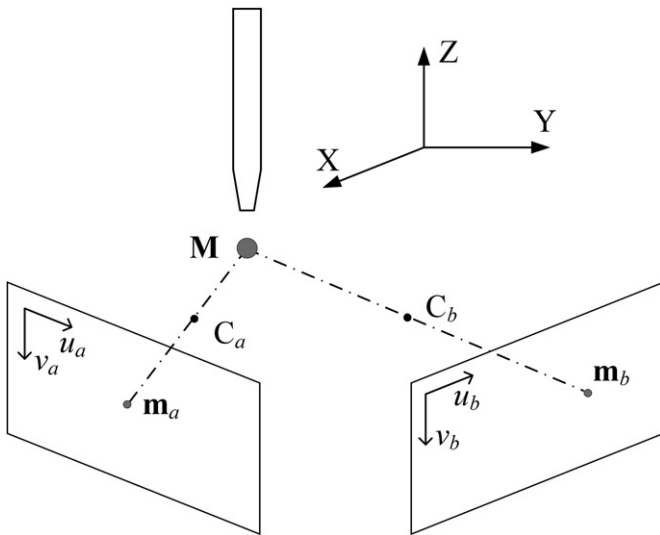


Figure 3. Pinhole camera stereo model.

information of the camera. In the proposed 3D printing application, advantage can be taken of high-accuracy 3-axis stages to scan the scene space and naturally incorporate it into the calibration system, which can significantly simplify the calibration and detection process and reduce computational cost. The details will be discussed in Section 2.2.2.

The pinhole model (Faugeras, 1993) is used in the proposed catadioptric stereo system. For the sake of simplicity, one camera is used as an example to explain the formulation of the catadioptric stereo model, and the same procedure can be directly applied to another camera. As shown in Figure 3, $\mathbf{M} = [X, Y, Z, 1]^T$ is used to represent a droplet's location in the 3D printer, which also defines the world coordinate of the whole system. C_a and C_b are the center locations of the real and virtual camera. $\mathbf{m}_a = [u_a, v_a, 1]^T$ and $\mathbf{m}_b = [u_b, v_b, 1]^T$ are the locations of the droplet in the image coordinate of the corresponding cameras. From Hartley and Zisserman (2003), we can derive the relation between \mathbf{m}_a , \mathbf{m}_b , and \mathbf{M} as

$$\begin{cases} \rho_a \mathbf{m}_a = K_a R_a [I - C_a] \mathbf{M} \\ \rho_b \mathbf{m}_b = K_b R_b [I - C_b] \mathbf{M} \end{cases} \quad (1)$$

where ρ_a and ρ_b are scalar multipliers, K_a and K_b are the intrinsic camera parameters, R_a and R_b are the rotation matrices of the cameras, $P = K_a R_a [I - C_a]$ is a 3×4 matrix which is also called the camera projection matrix. The projection matrix for the virtual camera can be defined as $Q = K_b R_b [I - C_b]$. Following Equation (1), the corresponding relations for the real camera and the virtual camera can be written in the following equations:

$$\begin{cases} \rho_a [u_a, v_a, 1]^T = P [X, Y, Z, 1]^T \\ \rho_b [u_b, v_b, 1]^T = Q [X, Y, Z, 1]^T \end{cases} \quad (2)$$

2.2. Location detection algorithm

As inferred by Equation (2), the location detection process can be conducted in the following three steps.

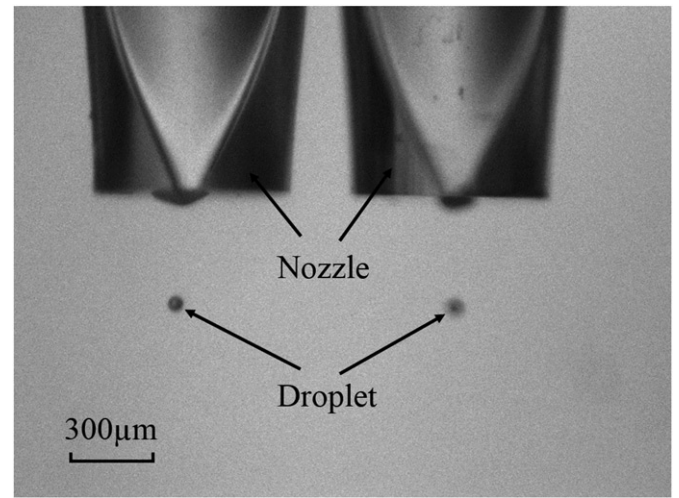


Figure 4. Image captured by the catadioptric stereo system. The nozzle and droplet on the left-hand side are directly captured by the camera, and the ones on the right-hand side are captured from the mirror using the same camera.

Step 1: Detect the droplet's center location in the image space for the two cameras, which are denoted as $[u_a, v_a]$ and $[u_b, v_b]$. A detailed discussion is presented in Section 2.2.1.

Step 2: Identify the projection matrices P and Q for the two cameras, which are obtained by scene calibration as is explained in Section 2.2.2.

Step 3: Solve Equation (2) to find the droplet location $[X, Y, Z]$ in world coordinate based on the location in image space (Step 1) and the projection matrices (Step 2). The detection algorithm is delineated in Section 2.2.3.

2.2.1. Detection of droplet location in the image space

A typical image of a droplet is shown in Figure 4. The stable droplet exhibits a spherical shape in the 3D world space and a disk shape in the corresponding 2D image space. The task of the detection of the location of the droplet in the image space can be converted to the problem of extracting the center point of the disk using an image processing approach. However, prior to the extraction of the center point, we observed that the virtual image (right-hand side image in Figure 4) is not sharply focused. This is attributed to the short focal-depth caused by the magnification lens. To address this problem, the image processing needs to provide a good estimation of the droplet centroid, even though it is not sharply focused.

The out-of-focus phenomenon has been studied in terms of various aspects (Asada *et al.*, 1998; Chen *et al.* 2015). In the defocusing process, the optical center always lies on the axis of the lens system, due to the round lens used in the proposed system. Based on the thin lens model, the contour of the defocused droplet is still a circle and the centroid of the blurred image is still on the line from C_a or C_b to the target \mathbf{M} . The defocusing process is illustrated in Figure 5. The target is placed at out-of-focus location \mathbf{M} , forming an expanded blurred image. The imaging process can be modeled by the following convolution operation:

$$im_b = f_k * im_o, \quad (3)$$

where im_b is the observed image, im_o is the corresponding sharp image, and the blurring filter f_k is a scaled version of

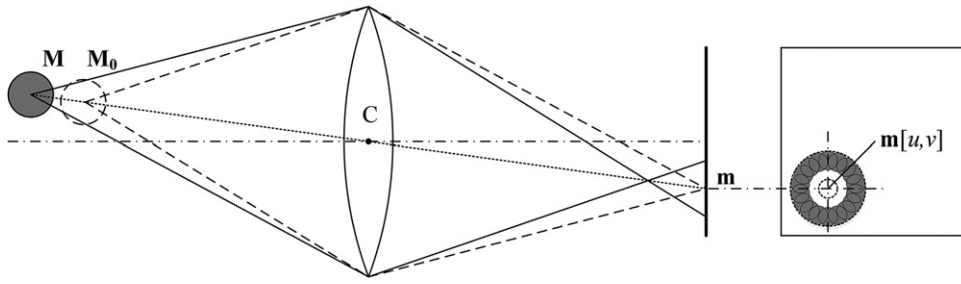


Figure 5. The influence of out-of-focus phenomena on the estimation of the center of the droplet.

the aperture shape (potentially convolved with the diffraction pattern) (Levin *et al.*, 2007). An out-of-focus point light source is imaged into a blurred circle, whose radius is described by a blurring parameter σ defined as

$$\sigma = \kappa r v \left(\frac{1}{f} - \frac{1}{v} - \frac{1}{u} \right), \quad (4)$$

where f is the focal length, u is the distance of the object point from the lens, v is the distance between the lens and the image detector, r is the radius of the lens aperture, and κ is a camera constant that depends on its optics and the CCD array resolution (Rajan and Chaudhuri, 2003). Nevertheless, the centroid of the blurred image (\mathbf{m}) overlaps the center of the target placed at the in-focus location \mathbf{M}_0 . It is noted that \mathbf{M} is on the line from \mathbf{m} to the optical center C , thus Equation (2) is still valid except that the value of ρ_a and/or ρ_b may change, which can be absorbed by the projection matrix discussed in Section 2.2.2.

The Hough transformation (Kimme *et al.*, 1975; Ballard, 1981) is widely used to identify location of a circle in an image. Our experimental results show that it can effectively locate the droplet. However it is computationally expensive, for example, it takes 0.3 seconds to process an image with 640×480 pixels on a typical laptop computer. Therefore, the Hough transformation is not suitable for high-efficiency online monitoring applications. In this work, we utilized a facile image binarization and centralization approach to efficiently and reliably detect the droplet location in the image space. We realized that after Gaussian filtering, the droplet image shows the same pattern despite the out-of-focus phenomena. Figure 6(a) shows the in-focus droplet (Figure 4 left), and Figure 6(b) shows the out-of-focus droplet (Figure 4 right). The image intensity shows a bell-shaped distribution, which agrees with previous research work (Zhang *et al.*, 2007). In this scenario, the droplet can be identified based on the circularity of the cross-section. In order to increase the reliability and accuracy, the image background (not covered by the droplet) noise level is examined, and its maximum intensity is found to be less than 10% of the peak value of the droplet area. Taking 50% of the peak value as the threshold, the droplet image can be separated from the background, and its location is detected as the center of the cross-section of the intensity distribution.

Previous studies have shown that a more accurate size estimation can be obtained based on the blurred image (Elder and Zucker, 1998; Chen *et al.*, 2015). However, our research only focuses on location detection, which is invariant of the level of blurring of the droplet image. Using reconstruction algorithms

based on the blurred images, the full information about the 3D droplet can be extracted by following a similar procedure, which will be studied in our future work.

2.2.2. Identification of the projection matrix by scene calibration

In order to establish the relation between the image location and the scene location, we need to know the camera matrices P and Q in Equation (2). As for a catadioptric stereo system, the camera matrices only depend on the camera itself and the relative location between the mirror and the camera. After calibration, the system can be used for droplet detection as long as the mirror is fixed relative to the camera. Several methods have been presented to obtain the camera matrix for a single camera system. In particular, Zhang's model (Sturm and Maybank, 1999; Zhang, 1999) is widely used for this purpose; it requires images of a chessboard captured from different angles. However, we realize it is a significant challenge to deploy the single camera calibration system in the droplet detection application, and it is more effective to calibrate the system integrated with camera and mirror as a whole. In the inkjet 3D printing system, droplet deviation typically happens in a very small range ($< 1 \text{ mm} \times 1 \text{ mm}$) and the resolution needs to be as high as $10 \mu\text{m}$, and thus a magnification lens or microscope system is used to detect the micro-scale droplet. Therefore it is difficult to obtain a tiny and accurate chessboard calibration plate suitable for this field of view. Even if such a calibration plate is available, the depth of field of a microscope is usually very small, making it very difficult to capture images from a wide variety of view angles, which is required by the traditional calibration algorithm. To address this challenge, we calibrate the catadioptric system as a whole. Specifically, an accurate X - Y - Z stage system is used for the calibration. In this case, the X - Y - Z coordinates of each target point can be directly read from the stage system and it also provides the ground truth for our evaluation experiments. In a 3D printing system, it is also possible to calibrate the system online, as most 3D printing systems have a precise motion control system, which can be used to provide accurate location information for the catadioptric stereo system.

The purpose of the calibration procedure is to obtain the camera matrices P and Q in Equation (2). As discussed above, the target location information \mathbf{M} can be obtained from the motion control system of the 3D printing system. The corresponding coordinates in the image space can be obtained by using an image processing approach described in Section 2.2.1. To solve the projection matrix, Equation (2) can be explicitly rewritten as follows with P_{ij} and Q_{ij} as

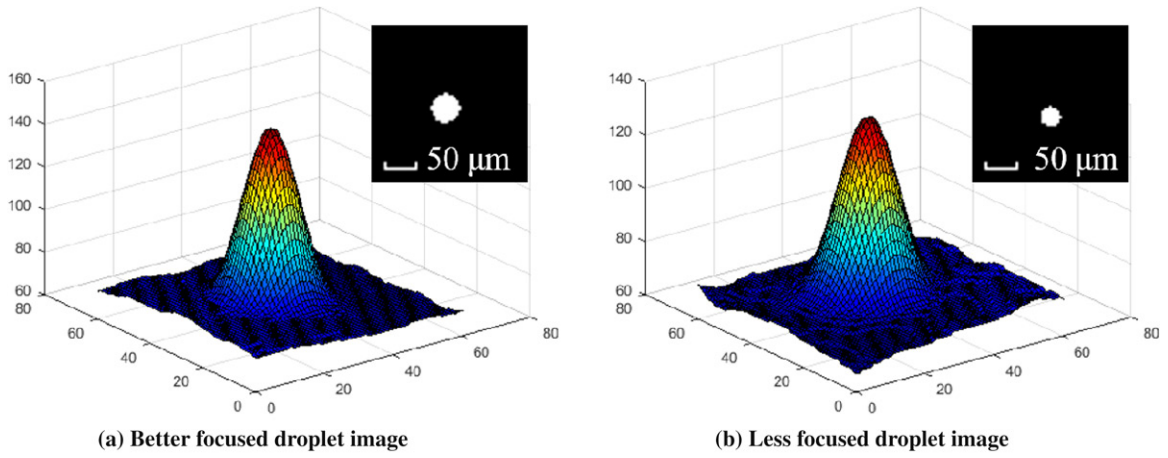


Figure 6. Surface plot of the grayscale value of the droplet image and the corresponding binarized image.

the elements of P and Q matrix respectively:

$$\begin{cases} \rho_a u_a = P_{11}X + P_{12}Y + P_{13}Z + P_{14} \textcircled{1} \\ \rho_a v_a = P_{21}X + P_{22}Y + P_{23}Z + P_{24} \textcircled{2} \text{ and} \\ \rho_a = P_{31}X + P_{32}Y + P_{33}Z + P_{34} \textcircled{3} \\ \rho_b u_b = Q_{11}X + Q_{12}Y + Q_{13}Z + Q_{14} \textcircled{4} \\ \rho_b v_b = Q_{21}X + Q_{22}Y + Q_{23}Z + Q_{24} \textcircled{5} . \\ \rho_b = Q_{31}X + Q_{32}Y + Q_{33}Z + Q_{34} \textcircled{6} \end{cases} \quad (5)$$

From these two groups of equations, the scale numbers ρ_a and ρ_b can be eliminated. For example, the following equation for the real camera can be derived from Equation (3):

$$\begin{cases} (P_{11}X + P_{12}Y + P_{13}Z + P_{14}) - u_a(P_{31}X + P_{32}Y + P_{33}Z + P_{34}) = 0 \\ (P_{21}X + P_{22}Y + P_{23}Z + P_{24}) - v_a(P_{31}X + P_{32}Y + P_{33}Z + P_{34}) = 0 \end{cases} \quad (6)$$

The camera matrix P and/or Q can be solved from the equation system by using the direct linear transformation algorithm (Hartley and Zisserman, 2003). Obviously, multiple target points are required for the calibration process to solve all the 12 elements of matrix P from the equation system. For each target point i , the image location from the real camera is denoted as $[u_{ai}, v_{ai}]$, and its world coordinate is $[X_i, Y_i, Z_i]$. If we define a vector $p = [P_{11}, P_{12}, P_{13}, P_{14}, P_{21}, P_{22}, P_{23}, P_{24}, P_{31}, P_{32}, P_{33}, P_{34}]^T$ and

$$\begin{cases} h_{ui} = [X_i, Y_i, Z_i, 1, 0, 0, 0, 0, -u_{ai}X_i, -u_{ai}Y_i, -u_{ai}Z_i, -u_{ai}] \\ h_{vi} = [0, 0, 0, 0, X_i, Y_i, Z_i, 1, -v_{ai}X_i, -v_{ai}Y_i, -v_{ai}Z_i, -v_{ai}] \end{cases}, \quad (7)$$

the equation for multiple target points can be written as:

$$\begin{bmatrix} h_{u1} \\ h_{v1} \\ \vdots \\ h_{ui} \\ h_{vi} \\ \vdots \end{bmatrix} p = Hp = 0, \quad (8)$$

where H is a $2n \times 12$ matrix, n is the total number of target points used in the calibration process. To solve p from the above homogeneous linear system, we need at least six target

points to provide 12 equations. However, due to the inevitable error in $[u_{ai}, v_{ai}]$ and $[X_i, Y_i, Z_i]$ introduced during the calibration process, it is more reliable to calibrate more than six target points to achieve a higher accuracy. As such, the original linear equation system is converted into the following optimization problem, which can be efficiently solved by using singular value decomposition:

$$\hat{p} = \arg \min_p \|Hp\|_2. \quad (9)$$

The optimal \hat{p} is a good estimation of the P matrix for the real camera. For the image obtained from the mirror, the same procedure can be followed to obtain the estimation of the Q matrix for the virtual camera.

2.2.3. Droplet location in the world space

In the previous two steps, we obtained the droplet location in the image spaces $[u_a, v_a]$ and $[u_b, v_b]$, and the camera projection matrices P and Q . The droplet location in the world space can be obtained from Equation (3) once the scalar multiplier ρ_a and ρ_b are available. Nevertheless, these scalar multipliers can be eliminated from the equation, and the following equation can be obtained after consolidation:

$$\begin{bmatrix} P_{31}u_a - P_{11} & P_{32}u_a - P_{12} & P_{33}u_a - P_{13} \\ P_{31}v_a - P_{21} & P_{32}v_a - P_{22} & P_{33}v_a - P_{23} \\ Q_{31}u_b - Q_{11} & Q_{32}u_b - Q_{12} & Q_{33}u_b - Q_{13} \\ Q_{31}v_b - Q_{21} & Q_{32}v_b - Q_{22} & Q_{33}v_b - Q_{23} \end{bmatrix} \begin{bmatrix} X \\ Y \\ Z \end{bmatrix} = \begin{bmatrix} P_{14} - P_{34}u_a \\ P_{24} - P_{34}v_a \\ Q_{14} - Q_{34}u_b \\ Q_{24} - Q_{34}v_b \end{bmatrix}. \quad (10)$$

This equation is a typical linear equation system, four linear equations with three unknowns define an overdetermined system, therefore the least squares solution of $[X, Y, Z]^T$ will be used as an estimation of the droplet location in the world space.

3. System implementation

3.1. System setup

We developed an integrated hardware and software system to test the proposed catadioptric stereo approach. The whole hardware setup is shown in Figure 7.

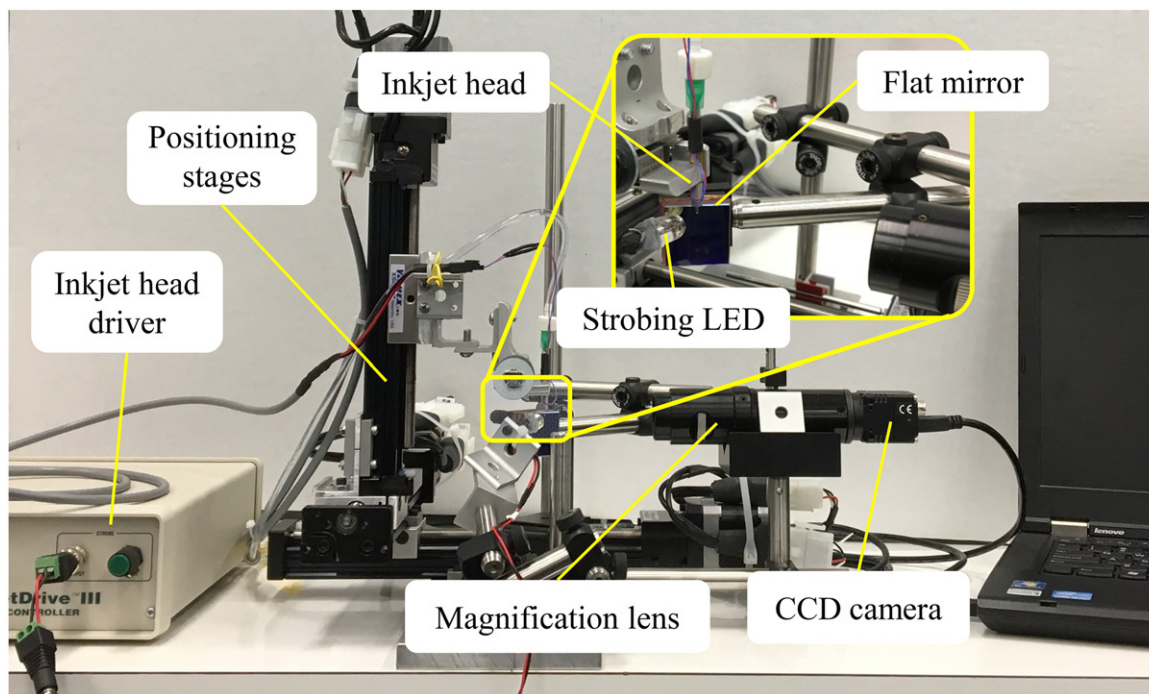


Figure 7. The setup of the catadioptric stereo system.

In this system, a piezo-based microdispensing nozzle (MicroFab Inc.) is used as the inkjet printhead with a printing rate of 100 to 1000 droplets/second. Typical Newtonian materials (deionized water and isopropyl alcohol) are used as the ink to test the printing and monitoring system, due to their excellent rheological properties favorable for inkjet printing. A CCD camera (Sensor Technologies Inc.) coupled with a strobing LED is used to capture the image of the jetted droplet. The image resolution is 640×480 pixels, and the camera communicates with the computer through USB protocol. The controlling signal for the strobing LED is synchronized with the signal for the piezo printhead, therefore a static and clear image will be captured for the stable inkjet printing process (Wang, Kwok & Zhou, 2017c). A flat mirror with a broadband coating is attached to an adjustable optical mount for precise angle adjustment to obtain the best field of view. Specifically, the angle of the mirror to the camera axis is endeavored to be set as 45° to achieve equal resolution in X and Y directions.

The 45° angle is chosen to achieve the best equal resolution in both X and Y directions. To better illustrate this, consider a simplified 2D arrangement where the target is located at the original point of the coordinates as shown in Figure 8. It is known that the points located on the line perpendicular to the camera axis have the best resolution, as this line is parallel to the image plane which is coplanar with the CCD surface in most cases. We use this line as a base to evaluate the resolution distribution in the target area. On the x -axis, the length of $1/\cos(\theta)$ will be projected to the baseline as a unit length, and on the y -axis, the length of $1/\sin(\theta)$ will be projected on the baseline. Therefore we can use $r_{rc}(\theta) = 1/\cos(\theta) + 1/\sin(\theta)$ to quantify the resolution of the real camera in this area, i.e., the smaller the value of $r_{rc}(\theta)$, the better resolution we can achieve. As the

system is symmetric, the virtual camera follows the same relation $r_{vc}(\theta) = 1/\cos(\theta) + 1/\sin(\theta)$. For a catadioptric system, we can use the average of the two cameras to qualify the resolution of the whole system as $r_{cs}(\theta) = \frac{1}{2}r_{rc}(\theta) + \frac{1}{2}r_{vc}(\theta) = 1/\cos(\theta) + 1/\sin(\theta)$. In this condition, we can easily find out the minimum value of $r_{cs}(\theta)$ can be obtained at $\theta = 45^\circ$. Further evaluation of $r_{cs}(\theta)$ showed that $r_{cs}(\theta)$ is small and insensitive to θ in the range between 30 and 45° . This implies that even though the angle is not accurately set as 45° , it will not have much influence on the overall resolution of the system.

The magnification lens system (MicroFab Inc.) is deployed to capture the tiny droplet with a narrow working range that only covers the allowable droplet locations. The inkjet head is mounted on an X - Y - Z stage system (Velmex Inc.) with straight-line accuracy of $0.001''/10''$ and screw lead accuracy of $0.003''/10''$ driven by stepper motors. This motion system provides micrometer-level accuracy, which is good enough for the camera calibration and system evaluation in the studies performed in this investigation. In the real-world implementation, the flat mirror, lens, and camera can be fixed together, and another reflection mirror can be added to change the location of the camera to increase the level of accessibility.

3.2. Detection range and calibration

The detection range is largely limited by the defocusing effect. To a certain extent, the out-of-focus phenomenon has no influence on the detection of the droplet. However, when the image is too blurry to locate the center of the droplet, the system reaches its detection range limit. As both the image directly captured by the camera and the image from the mirror need to be clear, an appropriate working range

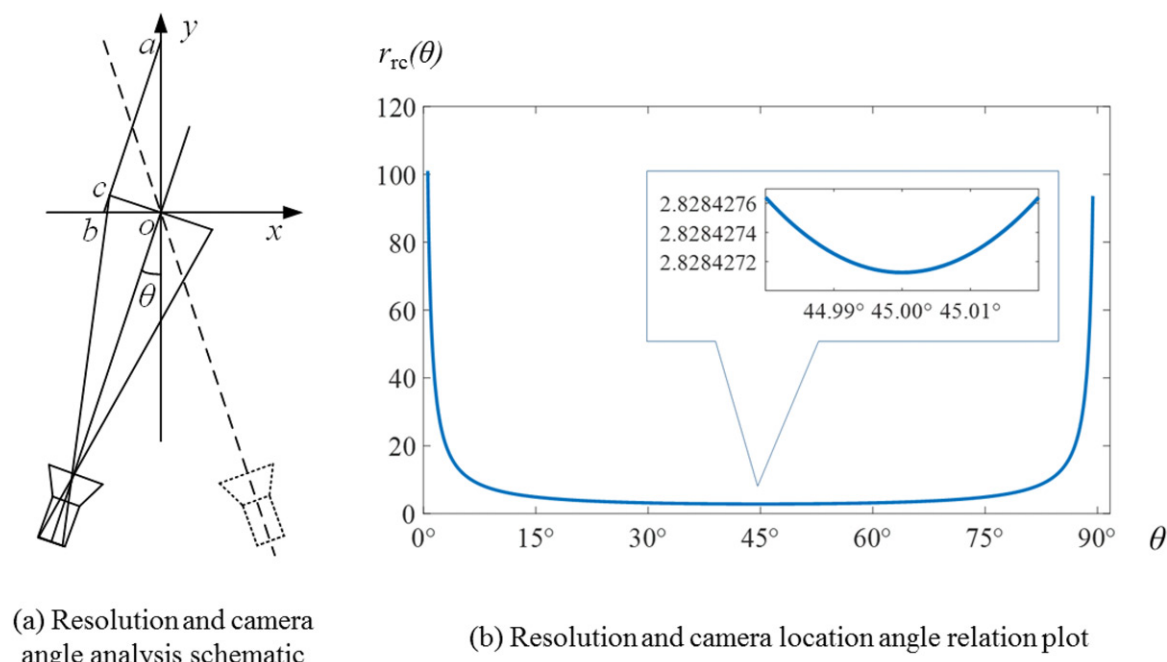


Figure 8. Resolution and camera angle analysis.

identified in the proposed system is in a $400 \mu\text{m} \times 400 \mu\text{m} \times 400 \mu\text{m}$ cubic space, which is good enough to detect deviations in the detection of the droplet.

The calibration process is carried out before droplet detection. In the cubic detection space, 27 boundary points (vertex of the cube, the middle point of edges and faces, and the center point) are selected as the target points for the calibration process. The x , y , and z coordinates of each calibration point can be read from the positioning stage system. Then three images at each calibration point are captured and the droplet location in the image space is detected by using the process discussed in Section 2.2.1. The average droplet location in the image space from three images is used to minimize the error. When all the droplet locations in the image space of the 27 calibration points are obtained, the camera matrices P and Q can be calculated by Equation (9). After calibration, the mirror and camera location and the focal length of the optical system are kept fixed during subsequent detection and monitoring processes.

4. System evaluation

In this section, the proposed catadioptric stereo system will be evaluated to verify whether it can address the fundamental challenges discussed in Section 1.2, and consequently achieve online droplet monitoring with high efficiency and accuracy. More specifically, the “accuracy” criterion will be evaluated by the system resolution and detection accuracy; the “efficiency” criterion will be evaluated by the computational and operational time cost both theoretically and experimentally; the “multi-dimensional information” criterion will be evaluated by checking whether the 3D information of multi-facet properties (location, speed, etc.) of the droplet can be effectively obtained. The detailed evaluation process is discussed in the following sections.

4.1. Resolution evaluation

High resolution is important to a droplet monitoring system in inkjet 3D printing. To exam the resolution of the proposed catadioptric system, we first evaluate the average resolution of the moving droplet in X and Y directions; the coordinate configuration is shown in Figure 1. The results in Figure 9(a) show that the resolution is relatively uniform on the X - Y plane. Figure 9(b) shows that the resolution in the Z -direction is much higher than the X and Y directions. This is due to the mirror being located perpendicular to the X - Y plane, when the droplet location changes in the Z -direction, both the real image and the virtual image will change, which gives better resolution based on our definition. The resolution difference between the X and Y axes is hypothetically caused by the angle of the mirror. As the mirror is not accurately located at exactly 45° to the X -axis, and the camera is more oriented along the X -axis, which gives better resolution in the orthogonal direction (along with the Y -axis). The average resolution on the X - Y plane is approximately $2.52 \mu\text{m}/\text{pixel}$; this is one order of magnitude higher than the printing system. Therefore, the proposed catadioptric system provides sufficient resolution for the monitoring of droplet location.

4.2. Accuracy evaluation

Compared with a single camera-based detection system, our dedicated catadioptric stereo system can provide accurate target location information in all three dimensions of the target area. With the help of the magnification lens, a high detection accuracy of the catadioptric system can be achieved. By focusing on a small detection range, more detailed information can be captured by the camera. In this section, the accuracy of the proposed catadioptric stereo system is evaluated.

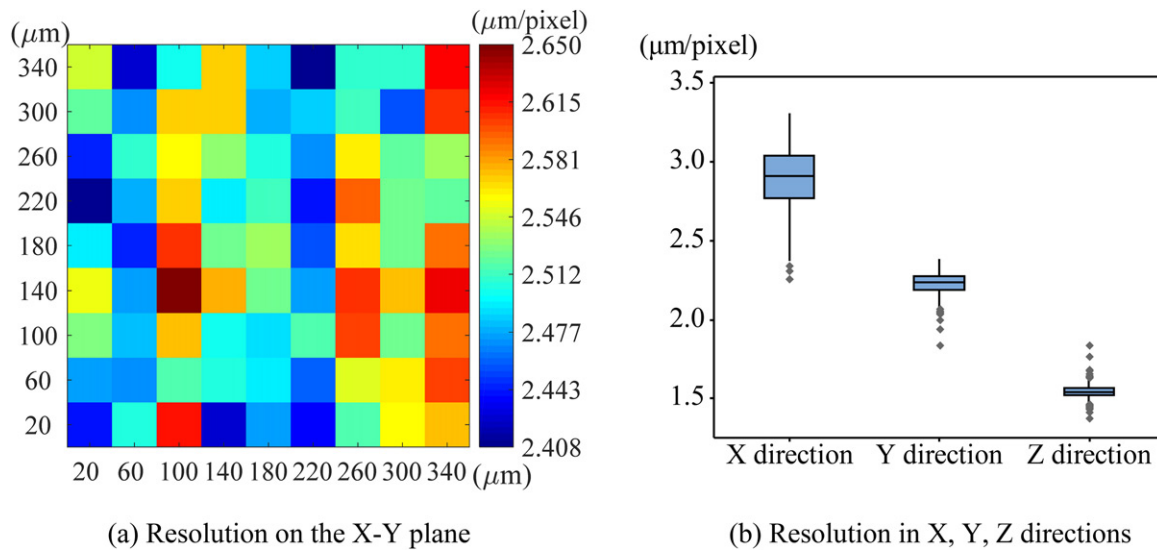


Figure 9. Resolution evaluation.

In the whole detection range of $400\ \mu\text{m} \times 400\ \mu\text{m} \times 400\ \mu\text{m}$ cubic space, 11 test points were selected in each dimension with a $40\text{-}\mu\text{m}$ distance between every two consecutive points. As the starting points are eliminated, due to the motion backlash issue, we assembled a total of $10^*10^*10 = 1000$ test points for the accuracy evaluation. As mentioned before, the location information provided by the X-Y-Z stage serves as the ground truth for evaluation, and the results of the detection error are shown in Figure 10.

These figures show that the average errors in all directions are very small. Specifically, it is less than $1\ \mu\text{m}$ in both the X and Y directions, and $-1\ \mu\text{m}$ in the Z-direction. The maximum error is within $\pm 10\ \mu\text{m}$ and the standard deviation is less than $2\ \mu\text{m}$ in each direction. The Euclidean distance between the true location and the detected result is evaluated, and the results in Figure 10(d) show that the average error is around $2.7\ \mu\text{m}$. It should be noted that the system accuracy of an inkjet printing process is in the range between 25 and $100\ \mu\text{m}$, thus the accuracy of the proposed monitoring system is one order of magnitude higher than the accuracy obtained in the 3D printing process. It is safe to conclude that the proposed catadioptric stereo system is suitable for droplet monitoring in inkjet printing application, and it has the potential to enable a closed-loop control system.

4.3. Time efficiency evaluation

Time efficiency plays another important role in the online monitoring system. As shown in Equation (10) of the mathematical model, the calculation of the location of a droplet has constant time complexity $O(1)$, which serves as the foundation to enable online monitoring application. We tested the computational performance of our catadioptric stereo system, the image size of each capture was 640×480 pixels, the algorithm was implemented in the Matlab environment, and the image transfer protocol from camera to PC is USB 2.0. The result is shown in Table 1, and the breakdown analysis is shown in Figure 11.

As shown in the results on the breakdown of the components of the process time (Figure 11), the image capture and

data transfer take up most of the processing time during each detection cycle. The process of the droplet location detection in the image space also takes around 20% of the total time, while the calculation from the image coordinate to real-world 3D printer coordinate takes a vanishingly small amount of time. The total processing time is around 50 ms (20 droplets can be detected per second), which is good enough for the less demanding applications in real-time. Nevertheless, the performance can be significantly improved in the following aspects:

1. Implement the algorithm using programs that can access system input/output (IO) much faster than the Matlab environment.
2. Use faster transfer protocols such as USB3.0 or Ethernet.
3. Replace the personal computer with embedded computing architectures such as a Digital Signal Processor to eliminate the data transfer process and drastically improve the time efficiency of the system.
4. Deploy parallel computing unit such as Field-Programmable Gate Array to significantly increase the image processing speed.

It is expected that the monitoring and detection time can be shortened to be within a single millisecond once the above-mentioned modules are integrated into the catadioptric stereo system. Therefore, the proposed technique is very promising to detect every single droplet and truly enable the online droplet monitoring for inkjet 3D printing process.

4.4. Droplet velocity detection

Based on the droplet location detection results, the droplet's velocity can be readily detected. As discussed in Section 3.1, the strobing system is used to capture the droplet image at a certain location determined by the synchronized control signal. Images at different locations can be captured by adjusting the delay time between the synchronized signals for the strobing LED and piezo printhead (Wang, Kwok & Zhou, 2017c). The droplet's velocity can be derived based on the

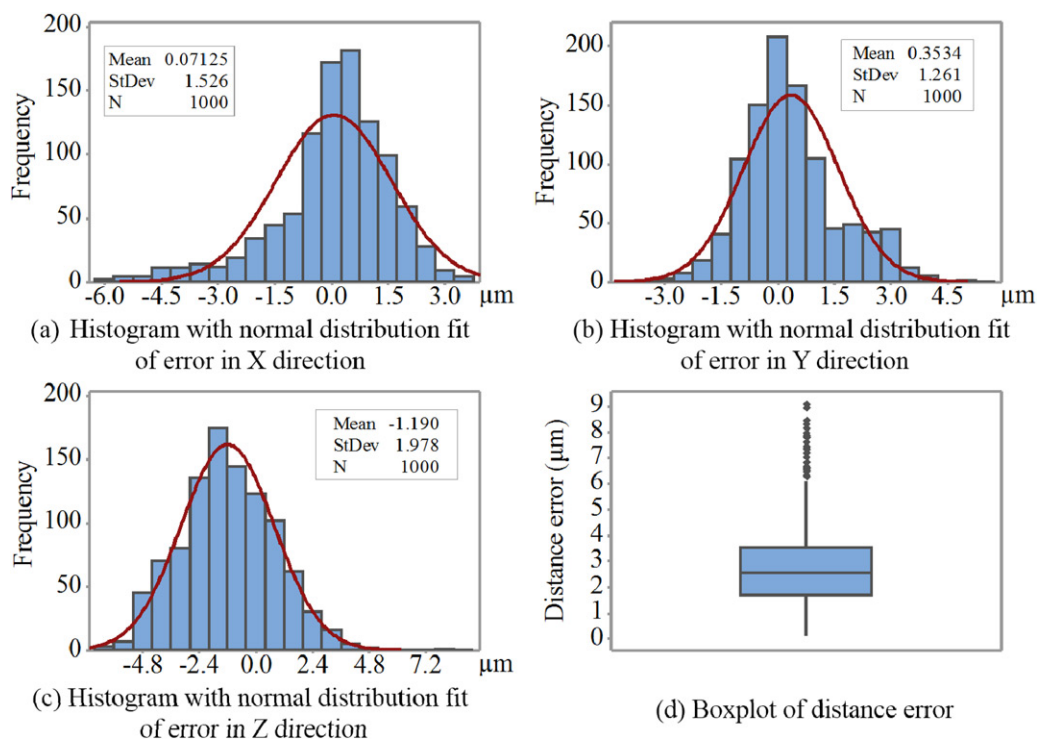


Figure 10. Histogram of error with normal distribution fitting.

Table 1. The computational cost of the monitoring system for one droplet (unit: s).

Image capture	Droplet detection in image	Droplet location calculation	Total time
0.0404	0.0107	4.028×10^{-5}	0.0511

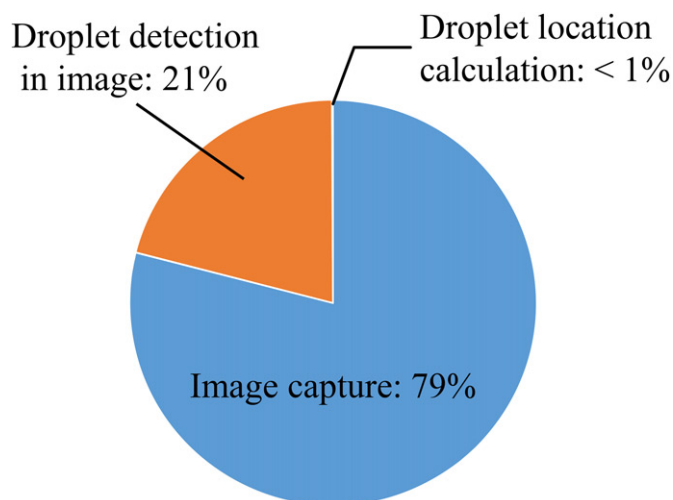


Figure 11. Breakdown of the process time for the detection of the location of a droplet.

distance between the two different locations and the corresponding delay time as follows:

$$V = \frac{1}{t_2 - t_1} \left(\begin{bmatrix} X_{t_2} \\ Y_{t_2} \\ Z_{t_2} \end{bmatrix} - \begin{bmatrix} X_{t_1} \\ Y_{t_1} \\ Z_{t_1} \end{bmatrix} \right), \quad (11)$$

where the V is the velocity of the droplet, $t_2 - t_1$ is the elapsed time between two different detected droplet-

locations at t_1 and t_2 , $[X_{t_1}, Y_{t_1}, Z_{t_1}]^T$ is the detected droplet location at t_1 and $[X_{t_2}, Y_{t_2}, Z_{t_2}]^T$ is the detected droplet location at t_2 . In our experiment, after the first droplet location was detected, the delay time of the strobe light was increased from $400 \mu\text{s}$ to $700 \mu\text{s}$. The droplet speed can be calculated as the difference of the droplet locations during the $300 \mu\text{s}$ period. To show the speed changes, we varied the drive voltage applied to the piezo printhead, from 40 V to 44 V , the relation between the droplet speed and the applied voltage is shown in Figure 12.

The velocity results (Figure 12) show the X , Y , Z components of the velocity vector. It is interesting to observe that the velocity in the X and Y directions is not obviously affected by the voltage change, whereas the velocity in the Z -direction proportionally increases when the drive voltage increases. This is because the increased drive voltage only increases the propelling force in the negative Z -direction; the reported results agree with those of a previously presented study (Erqiang, 2010) and technote presented by MicroFab Inc. (Wallace, 1999) very well.

4.5. Repeatability and reproducibility study

In order to assess the variation of the proposed catadioptric stereo detection system from a statistic perspective, crossed gauge repeatability and reproducibility (R&R) studies are performed. In this research, the detection process is fully controlled by the computer software, and thus the usability of designed software is not part of this research. On the other hand, the calibration process plays an important role and may introduce certain variations to the detection system; therefore we use the calibration operation as the factor of the reproducibility in our system evaluation.

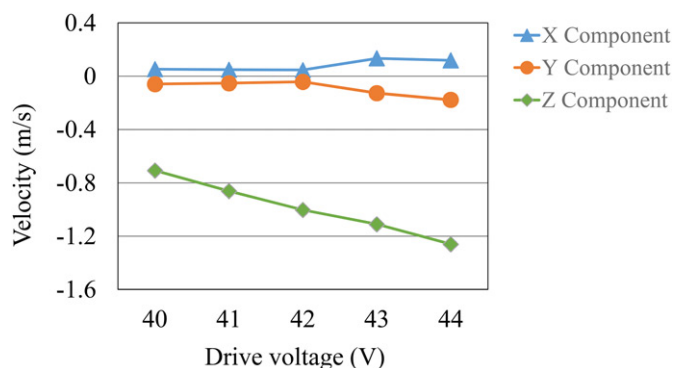


Figure 12. Detection of the velocity of the droplet.

In this study, three different calibration operations were processed and the corresponding calibration data was used to calculate droplet location at each test point. Five test points were selected along the X -axis in the detection area with the coordinates of 40, 50, 60, 70, 80 μm . Each test point was measured five times by using different calibration data, in total 75 data points were generated in this study.

The ANalysis Of VAriance (ANOVA) method was used in this study, and the results are shown in Table 2. It can be seen that the Test point location and Calibrate operation are both statistically significant in the model and there is no significant interaction between the Location and Calibrate operations. As the interaction term has a p -value larger than 0.05, it is removed in the following study.

Gauge R&R study results are shown in Figure 13. Figure 13(a) is a Components of variation graph that shows that the largest component of variation is from part-to-part variation, more detailed data are shown in Table 3. More than 99.9% of the contribution of variance is from the part-to-part variation. In Figure 13(b), which is the R chart by calibration operation, all points fall within the control limits, indicating that the calibration operation is consistent. Figure 13(c) is an Xbar Chart for Calibration operation and shows that most of the points fall beyond the control limits, indicating that the collected data points represent the part-to-part variability. Figure 13(d) shows Detection data by location for each test point, and highlights that the detection results are close together with very small variation. Figure 13(e) shows a plot of Data by Calibration operation, it highlights that differences between calibration operations are small. In Figure 13(f) is the Location * Calibration operation Interaction graph, the lines connecting the detection results are close to each other, indicating that the detection results do not depend on the location from each calibration operation.

This study showed a good repeatability and reproducibility under the given situation; however, we are more interested in the relative variation in the catadioptric stereo system under different detection requirements. We performed more R&R studies with different selected test points that had different location variance (or standard deviation) along each coordinate axis, and used the percentage of the contribution of variance components to assess the detection system; the results are summarized in Table 4. In each case, five test points were selected and the detected locations were

Table 2. Two-way ANOVA table.

Source	DF	SS	MS	F	P
Test point location	4	13 833.5	3458.37	45 404.4	<0.001
Calibrate operation	2	4.0	2.01	26.4	<0.001
Location * Calibrate operation	8	0.6	0.08	1.1	0.354
Repeatability	60	4.0	0.07		
Total	74	13 842.1			

calculated based on three different calibration data. At each test point, the detection was performed five times. It can be seen that in the case of test points with a standard deviation of 7.21 μm in their location if these variances are along the X or Y axis, they will contribute more than 99% of the total variance; this becomes more than 82% if they are along the Z -axis. When the standard deviation is larger than 21.65 μm , the variance in all the three directions contributes more than 99% of the total variation. The comparison of different directions shows more R&R variance in the Z -direction, which agrees with the previous study in Section 4.1. This is because the system has a higher resolution in the Z -direction, more variance or noise in the detection process will be introduced to the final detection result.

Working environment study: We also evaluated the system performance under two different illumination conditions: (i) a light level of approximately 307 lux; and (ii) a light level of approximately 0 lux (no light). The system showed no difference in the detection performance. The main reason for this observation is that we use a strobe system to provide the light to capture the droplet image, only a very small amount of environmental light can be captured by the camera, as it has a very small view angle (approximately 1°).

5. Conclusions and future work

In this article, a catadioptric stereo system is proposed to online monitor the location of a droplet in an inkjet 3D printing process. In this system, a CCD camera is coupled with a flat mirror and magnification lens system to capture droplet images at different angles to detect the location of the droplet in 3D space. A mathematical model was formulated to map the location of the droplet in 3D world space and 2D image space. Specifically, a fast image processing algorithm was utilized to capture the droplet's location in image space and an efficient calibration procedure, by using the precise X - Y - Z stages, is proposed to accurately detect the droplet's location. A holistic hardware and software framework was constructed for the catadioptric stereo system. The performance of the proposed system was evaluated in terms of resolution, accuracy, efficiency, and versatility, both theoretically and experimentally. The results showed that the proposed catadioptric stereo system can achieve single micron resolution and accuracy, which is one-order-of-magnitude higher than the 3D printing system itself. The proposed droplet location detection algorithm has low time complexity $O(1)$, and the computational and operational time cost can be dramatically reduced by integrating advanced hardware modules, with the potential to detect one droplet in a single millisecond. Multi-facet features

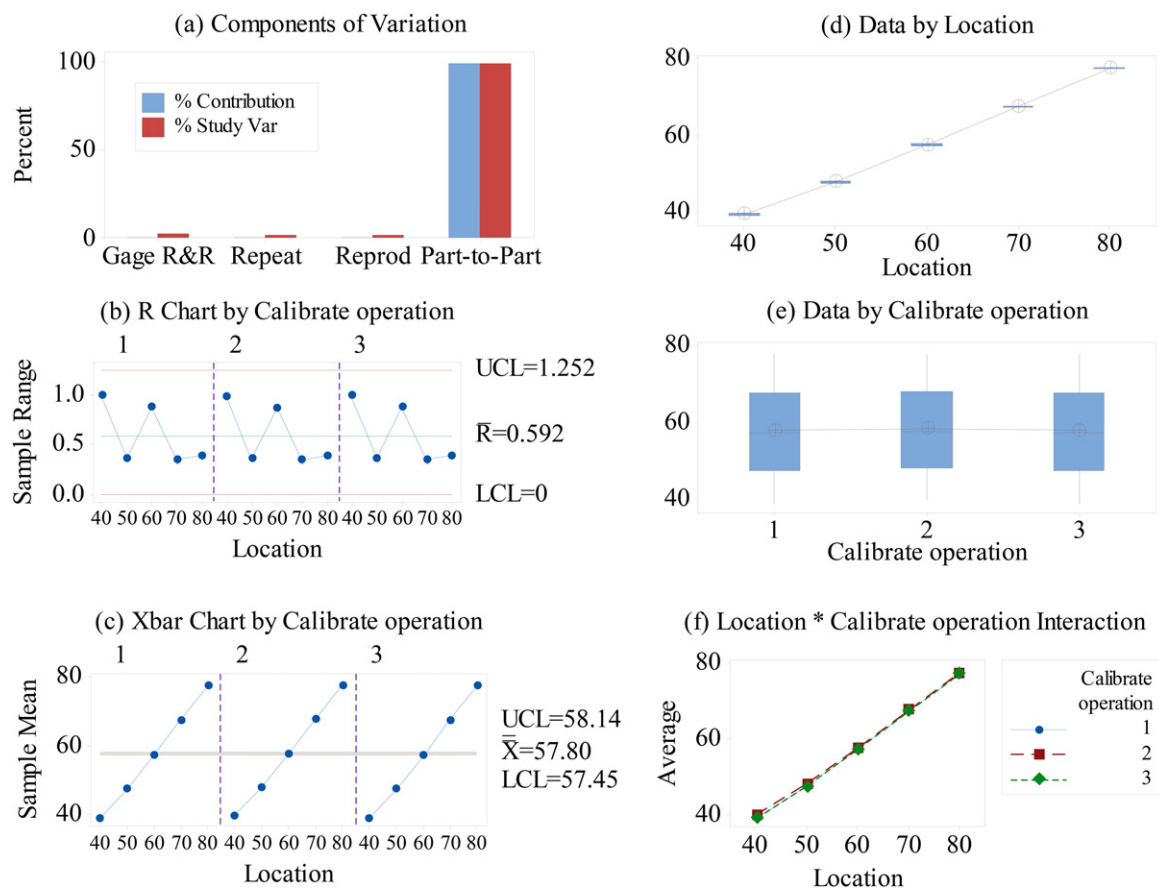


Figure 13. Gauge R&R Study.

Table 3. Gauge R&R variance components and gauge evaluation.

Source	Variance Components	% Contribution of Variance Components	Standard Deviation	% Contribution of Study Variance
Total Gauge R&R	0.146	0.06	0.3820	2.51
Repeatability	0.068	0.03	0.2611	1.72
Reproducibility (Calibrate operation)	0.078	0.03	0.2788	1.84
Part-To-Part	230.553	99.94	15.1840	99.97
Total Variation	230.699	100.00	15.1888	100.00

Table 4. Contribution of variance components (%) case study.

Study Case	#1 (StDev = 7.21 μm)			#2 (StDev = 14.43 μm)			#3 (StDev = 21.65 μm)		
	X	Y	Z	X	Y	Z	X	Y	Z
Total Gauge R&R	0.41	0.09	17.71	0.06	0.04	2.88	0.03	0.02	0.97
Part-To-Part	99.59	99.91	82.29	99.94	99.96	97.12	99.97	99.98	99.03

including the droplet location and speed can be effectively detected by the proposed technique. In conclusion, the proposed catadioptric stereo system is very promising for online droplet monitoring and has tremendous potential to enable trustworthy quality assurance in inkjet 3D printing.

This article, for the first time, presents a catadioptric stereo system for droplet monitoring and detection in 3D printing applications. Future research work includes:

1. Droplet size detection. The size is another important feature of the droplet and significantly affects the process and product quality. The major challenge in

extending the proposed work to size detection is still the out-of-focus issue. However, based on the droplet location detected in this work, the defocusing effect can be captured (Elder and Zucker, 1998; Hasinoff and Kutulakos, 2011; Chen *et al.*, 2015) and better estimation of the droplet size can be obtained;

2. Feedback control system. By monitoring the droplet location and fly speed in inkjet 3D printing process, the landing location of the jetting droplets can be predicted, with the help of closed-loop control or decision-making system, the mislanding problem of the droplets can be avoided to improve the printing quality.

Funding

The authors gratefully appreciate the financial support from the National Science Foundation (NSF) through CNS-1547167, the seed fund support from Center of Excellence in Materials Informatics and Sustainable Manufacturing and Advanced Robotics Technology (SMART) Community of Excellence program at the University at Buffalo.

Notes on Contributors

Tianjiao Wang is a Ph.D. candidate in the Department of Industrial and Systems Engineering at the University at Buffalo, SUNY. He received his bachelor's (2010) and master's (2012) degrees in electronic engineering from Harbin Institute of Technology, and he worked as a system design engineer in Beijing A&E Technology Co., thereafter. His current research focuses on innovative additive manufacturing process and manufacturing data analytics.

Chi Zhou is an assistant professor in the Department of Industrial and Systems Engineering at the University at Buffalo (UB). He received his doctorate in industrial and systems engineering from the University of Southern California in 2012. Prior to joining UB in July 2013, he was a senior research and development engineer at EnvisionTec Inc. His current research interests are in the areas of computer-aided design and manufacturing (CAD/CAM) related to direct digital manufacturing. He has received several best paper awards in SME and ASME-related conferences and journals. He is also the recipient of 2014 Outstanding Young Manufacturing Engineer from SME and Young Investigator Award from UB.

Wenyao Xu received a Ph.D. degree from the University of California, Los Angeles, CA, USA, in 2013. He received both an M.S. degree in 2008 and a B.S. degree in 2006 from Zhejiang University, China (both with honor). Currently, he is an associate professor in the Computer Science and Engineering Department, the State University of New York (SUNY) at Buffalo. He has published over 140 technical papers, co-authored two books, and is a named inventor on many International and U.S. patents. His recent research foci include Internet of things, smart health and cyber-physical security, and his work has received six Best Paper Awards in related research fields.

ORCID

Tianjiao Wang  <http://orcid.org/0000-0003-1152-9535>

Chi Zhou  <http://orcid.org/0000-0001-7230-3754>

Wenyao Xu  <http://orcid.org/0000-0001-6444-9411>

References

- Ammi, M., Fremont, V. and Ferreira, A. (2005) Flexible microscope calibration using virtual pattern for 3-d telemicromanipulation, in *Proceedings of the 2005 IEEE International Conference on Robotics and Automation*, IEEE Press, Piscataway, NJ, pp. 3888–3893.
- Asada, N., Fujiwara, H. and Matsuyama, T. (1998) Analysis of photometric properties of occluding edges by the reversed projection blurring model. *IEEE Transactions on Pattern Analysis and Machine Intelligence*, **20**, 155–167.
- Ballard, D.H. (1981) Generalizing the Hough transform to detect arbitrary shapes. *Pattern Recognition*, **13**, 111–122.
- Bose, S., Vahabzadeh, S. and Bandyopadhyay, A. (2013) Bone tissue engineering using 3D printing. *Materials Today*, **16**, 496–504.
- Chen, C.-H., Zhou, H. and Ahonen, T. (2015) Blur-aware disparity estimation from defocused stereo images, in *Proceedings of the IEEE International Conference on Computer Vision*, IEEE Press, Piscataway, NJ, pp. 855–863.
- Chen, Y., Li, K. and Qian, X. (2013) Direct geometry processing for telefabrication. *Journal of Computing and Information Science in Engineering*, **13**, 041002–041020.
- Cheng, Y. and Jafari, M.A. (2008) Vision-based online process control in manufacturing applications. *IEEE Transactions on Automation Science and Engineering*, **5**, 140–153.
- Elder, J.H. and Zucker, S.W. (1998) Local scale control for edge detection and blur estimation. *IEEE Transactions on Pattern Analysis and Machine Intelligence*, **20**, 699–716.
- Erqiang, L. (2010) The generation and experimental study of micro-scale droplets in drop-on-demand inkjet printing, Doctoral dissertation, Xi'an Jiaotong University. Available at <https://scholarbank.nus.edu.sg/bitstream/10635/22832/1/LIEQ.pdf>.
- Faes, M., Abbeloos, W., Vogeler, F., Valkenaers, H., Coppens, K., Goedemé, T. and Ferraris, E. (2016) Process monitoring of extrusion based 3D printing via laser scanning. *arXiv preprint arXiv:1612.02219*.
- Faugeras, O. (1993) *Three-Dimensional Computer Vision: A Geometric Viewpoint*, MIT Press, Cambridge, MA.
- Favaro, P., Mennucci, A. and Soatto, S. (2003) Observing shape from defocused images. *International Journal of Computer Vision*, **52**, 25–43.
- Figl, M., Ede, C., Hummel, J., Wanschitz, F., Ewers, R., Bergmann, H. and Birkfellner, W. (2005) A fully automated calibration method for an optical see-through head-mounted operating microscope with variable zoom and focus. *IEEE Transactions on Medical Imaging*, **24**, 1492–1499.
- Gao, F. and Sonin, A.A. (1994) Precise deposition of molten micro-drops: The physics of digital microfabrication. *Proceedings of the Royal Society of London A*, **444**, 533–554.
- Gao, W., Zhang, Y., Ramanujan, D., Ramani, K., Chen, Y., Williams, C.B., Wang, C.C., Shin, Y.C., Zhang, S. and Zavattieri, P.D. (2015) The status, challenges, and future of additive manufacturing in engineering. *Computer-aided Design*, **69**, 65–89.
- Gibson, I., Rosen, D.W. and Stucker, B. (2010) Design for additive manufacturing. In *Additive Manufacturing Technologies*, pp. 299–332. Springer, Boston, MA.
- Gluckman, J. and Nayar, S.K. (1999) Planar catadioptric stereo: Geometry and calibration, in *IEEE Computer Society Conference on Computer Vision and Pattern Recognition*, IEEE Press, Piscataway, NJ, pp. 22–28.
- Gluckman, J. and Nayar, S.K. (2002) Rectified catadioptric stereo sensors. *IEEE Transactions on Pattern Analysis and Machine Intelligence*, **24**, 224–236.
- Goshtasby, A. and Gruver, W.A. (1993) Design of a single-lens stereo camera system. *Pattern Recognition*, **26**, 923–937.
- Hartley, R. and Zisserman, A. (2003) *Multiple View Geometry in Computer Vision*, Cambridge University Press, New York, NY.
- Hasinoff, S.W. and Kutulakos, K.N. (2011) Light-efficient photography. *IEEE Transactions on Pattern Analysis and Machine Intelligence*, **33**, 2203–2214.
- Hu, D. and Kovacevic, R. (2003) Sensing, modeling and control for laser-based additive manufacturing. *International Journal of Machine Tools and Manufacture*, **43**, 51–60.
- Huang, Q. (2016) Systems and methods for predicting and improving scanning geometric accuracy for 3d scanners, US Patent Application No. 15/098,267.
- Inaba, M., Hara, T. and Inoue, H. (1993) A stereo viewer based on a single camera with view-control mechanisms, in *Proceedings of the 1993 IEEE/RSJ International Conference on Intelligent Robots and Systems*, IEEE Press, Piscataway NJ, pp. 1857–1865.
- Jackson, R.C., Liu, T. and Çavuşoğlu, M.C. (2016) Catadioptric stereo tracking for three dimensional shape measurement of MRI guided catheters, in *Proceedings of the IEEE International Conference on Robotics and Automation*, IEEE Press, Piscataway, NJ, pp. 4422–4428.
- Kimme, C., Ballard, D. and Sklansky, J. (1975) Finding circles by an array of accumulators. *Communications of the ACM*, **18**, 120–122.

- Levin, A., Fergus, R., Durand, F. and Freeman, W.T. (2007) Image and depth from a conventional camera with a coded aperture. *ACM Transactions on Graphics*, **26**, 70.
- Liu, C., Roberson, D. and Kong, Z. (2017) Textural analysis-based online closed-loop quality control for additive manufacturing processes, in *Proceedings of the IIE Annual Conference*, 20–23 May, Pittsburgh, PA, USA. Institute of Industrial and Systems Engineers (IISE), pp. 1127–1132.
- Mazumder, J., Dutta, D., Kikuchi, N. and Ghosh, A. (2000) Closed loop direct metal deposition: art to part. *Optics and Lasers in Engineering*, **34**, 397–414.
- Mazumder, J. and Voelkel, D.D. (1995) Method and apparatus for non-contact surface contour measurement, US. Patent No. is 5,446,549.
- Mironov, V., Boland, T., Trusk, T., Forgacs, G. and Markwald, R.R. (2003) Organ printing: Computer-aided jet-based 3D tissue engineering. *Trends in Biotechnology*, **21**, 157–161.
- Nene, S.A. and Nayar, S.K. (1998) Stereo with mirrors, in *Proceedings of the Sixth International Conference on Computer Vision*, IEEE Press, Piscataway, NJ, pp. 1087–1094.
- Potter, G. (2017) Vader systems may have created a quantum leap in manufacturing – Liquid metal 3-D printing could revolutionize how things are made. Available at <http://www.buffalo.edu/news/releases/2017/01/020.html>
- Rajagopalan, A. and Chaudhuri, S. (1997) A variational approach to recovering depth from defocused images. *IEEE Transactions on Pattern Analysis and Machine Intelligence*, **19**, 1158–1164.
- Rajan, D. and Chaudhuri, S. (2003) Simultaneous estimation of super-resolved scene and depth map from low resolution defocused observations. *IEEE Transactions on Pattern Analysis and Machine Intelligence*, **25**, 1102–1117.
- Ralis, S.J., Vikramaditya, B. and Nelson, B.J. (2000) Micropositioning of a weakly calibrated microassembly system using coarse-to-fine visual servoing strategies. *IEEE Transactions on Electronics Packaging Manufacturing*, **23**, 123–131.
- Rao, P.K., Liu, J., Roberson, D., Kong, Z. and Williams, C. (2015) Online real-time quality monitoring in additive manufacturing processes using heterogeneous sensors. *Journal of Manufacturing Science and Engineering*, **137**, 061007–61019.
- Salehi, D. and Brandt, M. (2006) Melt pool temperature control using LabVIEW in Nd: YAG laser blown powder cladding process. *The International Journal of Advanced Manufacturing Technology*, **29**, 273–278.
- Sturm, P.F. and Maybank, S.J. (1999) On plane-based camera calibration: A general algorithm, singularities, applications, in *Proceedings of the IEEE Computer Society Conference on Computer Vision and Pattern Recognition*, IEEE Press, Piscataway, NJ, pp. 432–437.
- Sun, H., Rao, P.K., Kong, Z.J., Deng, X. and Jin, R. (2018) Functional quantitative and qualitative models for quality modeling in a fused deposition modeling process. *IEEE Transactions on Automation Science and Engineering*, **15**(1), 393–403.
- Tootooni, M.S., Dsouza, A., Donovan, R., Rao, P.K., Kong, Z.J. and Borgesen, P. (2017) Classifying the dimensional variation in additive manufactured parts from laser-scanned three-dimensional point cloud data using machine learning approaches. *Journal of Manufacturing Science and Engineering*, **139**, 091005–091019.
- Toyserkani, E. and Khajepour, A. (2006) A mechatronics approach to laser powder deposition process. *Mechatronics*, **16**, 631–641.
- Wallace, D. (1999) Drive waveform effects on ink-jet device performance, MicroFab Technote, (1999) 3 Manning HJ, Harvey RA, Xaar greyscale technology. In *IS&T NIP25: International Conference on digital printing technology*, 17–22 October, Society for Imaging Science and Technology (IS&T).
- Wang, A., Song, S., Huang, Q. and Tsung, F. (2017a) In-plane shape-deviation modeling and compensation for fused deposition modeling processes. *IEEE Transactions on Automation Science and Engineering*, **14**, 968–976.
- Wang, A., Wang, T., Zhou, C. and Xu, W. (2017b) LuBan: Low-cost and in-situ droplet micro-sensing for inkjet 3D printing quality assurance, in *Proceedings of the 15th ACM Conference on Embedded Network Sensor Systems*, Delft, Netherlands, 6–8 November, Article no. 27. doi:10.1145/3131672.3131686.
- Wang, T., Kwok, T.-H. and Zhou, C. (2017c) In-situ droplet inspection and control system for liquid metal jet 3D printing process. *Procedia Manufacturing*, **10**, 968–981.
- Wang, T., Kwok, T.-H., Zhou, C. and Vader, S. (2018) In-situ droplet inspection and closed-loop control system using machine learning for liquid metal jet printing. *Journal of Manufacturing Systems*, **47**, 83–92.
- Wohlers, T. (2016) *Wohlers Report 2016*, Wohlers Associates, Inc., Fort Collins, CO.
- Xu, K. and Chen, Y. (2017) Photocuring temperature study for curl distortion control in projection-based stereolithography. *Journal of Manufacturing Science and Engineering*, **139**, 021002–021016.
- Xu, K., Kwok, T.-H., Zhao, Z. and Chen, Y. (2017) A reverse compensation framework for shape deformation control in additive manufacturing. *Journal of Computing and Information Science in Engineering*, **17**, 021012–021021.
- Yan, P., Brown, E., Su, Q., Li, J., Wang, J., Xu, C., Zhou, C. and Lin, D. (2017) 3D Printing hierarchical silver nanowire aerogel with highly compressive resilience and tensile elongation through tunable Poisson's ratio. *Small*, **13**, 1701756–1701763.
- Zhang, B., Zerubia, J. and Olivo-Marin, J.-C. (2007) Gaussian approximations of fluorescence microscope point-spread function models. *Applied Optics*, **46**, 1819–1829.
- Zhang, F., Yang, F., Lin, D. and Zhou, C. (2017) Parameter study of three-dimensional printing graphene oxide based on directional freezing. *Journal of Manufacturing Science and Engineering*, **139**, 031016.
- Zhang, Q., Zhang, F., Medarametla, S.P., Li, H., Zhou, C. and Lin, D. (2016) 3D printing of graphene aerogels. *Small*, **12**, 1702–1708.
- Zhang, Z. (1999) Flexible camera calibration by viewing a plane from unknown orientations, in *Proceedings of the Seventh IEEE International Conference on Computer Vision*, IEEE Press, Piscataway, NJ, pp. 666–673.
- Zhou, C. and Chen, Y. (2009) Calibrating large-area mask projection stereolithography for its accuracy and resolution improvements. Presented at the Solid Freeform Fabrication Symposium, Austin, TX.
- Zhou, C. and Chen, Y. (2009a) Three-dimensional digital halftoning for layered manufacturing based on droplets. *Transactions of the North American Manufacturing Research Institution of SME*, **37**, 175–182.
- Zhou, C., Chen, Y. and Waltz, R.A. (2009) Optimized mask image projection for solid freeform fabrication. *Journal of Manufacturing Science and Engineering*, **131**, 061004–061016.
- Zhou, C., Chen, Y., Yang, Z. and Khoshnevis, B. (2013) Digital material fabrication using mask-image-projection-based stereolithography. *Rapid Prototyping Journal*, **19**, 153–165.